Accurate method for determining adhesion of cantilever beams

M. P. de Boer[a)]
Intelligent Micromachining, Department 1725, MS 1080, Sandia National Laboratories, Albuquerque, New Mexico 87185

T. A. Michalske[b)]
Surface and Interface Science, Department 1114, MS 1413, Sandia National Laboratories, Albuquerque, New Mexico 87185

(Received 29 December 1998; accepted for publication 5 April 1999)

Using surface micromachined samples, we demonstrate the accurate measurement of cantilever beam adhesion by using test structures which are adhered over long attachment lengths. We show that this configuration has a deep energy well, such that a fracture equilibrium is easily reached. When compared to the commonly used method of determining the shortest attached beam, the present method is much less sensitive to variations in surface topography or to details of capillary drying. [S0021-8979(99)00414-4]

I. INTRODUCTION

Microelectrochemical Systems or MEMS (Ref. 1) are now being used in selected commercial products including airbag accelerometers for automobiles[2] and active optical elements[3] for projection displays. Due to their potential for low-cost manufacturing, many other microdevice designs and applications are currently being developed. Microrelays,[4] gyros,[5] optical switches,[6] and security devices[7] are just a few examples. However, autoadhesion, or spontaneous sticking between MEMS structures, remains a major limitation in bringing this new class of engineering devices to the broader market. MEMS are particularly susceptible to autoadhesion because the structural members: (1) are constructed in close proximity to each other (within several μms); (2) are highly compliant due to their extreme length-to-thickness aspect ratio; and (3) have large surface-to-volume ratios which increase the relative importance of adhesive surface forces. If the miniature structural members are brought together by surface (capillary, electrostatic) or inertial (shock, rapid air flow) forces, they may remain adhered after the external force is removed. Autoadhesion can lead to catastrophic failure of a MEMS device.

From a practical point of view, autoadhesion is known to limit manufacturing yield of silicon-based, surface micromachined MEMS. In these devices, structural members are fabricated using successively patterned depositions of thin-film polycrystalline silicon (polysilicon) and sacrificial oxide layers. This manufacturing approach is a direct outgrowth of silicon-based microelectronics. Autoadhesion can occur during the final step of surface micromachine fabrication after the polysilicon structural elements are rendered mechanically free by selectively etching away the sacrificial oxide layers in a hydrofluoric acid solution, which does not dissolve the polysilicon. During the final stage of drying from the wet etch, capillary menisci form between the released beams and the substrate and can generate forces that collapse the structural member onto the substrate. Subsequently, the polysilicon material may remain adhered to the substrate after the water dries. The problem is also commonly referred to as ''stiction.'' Numerous efforts have been directed at measuring autoadhesion and correlating to chemistry or roughness of the interface.[8–19] A supercritical drying procedure can be used to eliminate capillary forces during drying and prevent surfaces from coming into contact initially.[20] However, this approach does not address autoadhesion of surfaces that come into contact while devices are in operation. Many coating processes aimed at reducing the surface energy of polysilicon have also been explored.[8,21–23] Even though some of these coating strategies, particularly those based on silane coupling agents, have shown some promise for improving manufacturing yield and MEMS performance, their optimization requires a quantitative approach for measuring surface energy directly on micromachined devices. The interacting effects of coating material, roughness, and environmental aging on adhesion and friction must be understood in order to guarantee that the effect of surfaces forces on performance and reliability of micromachines will allow proper operations of devices over their lifetimes.

A theory and experimental method for measuring surface energy of micromachined cantilever beams has been proposed by Mastrangelo and Hsu.[10–12] They model the role of capillary forces in bringing beams into contact with the substrate and determine critical beam lengths for beam collapse.[11] As drying continues, the capillary volume diminishes leaving only surface-driven interfacial adhesion. Adhesion of the dried cantilever beam is predicted by considering the elastic energy in the deformed beam, which is attempting to pull the beam up off the substrate, and the surface energy that is promoting continued adhesion. By considering these two factors, Mastrangelo and Hsu calculated peel bounds[12] and the adhered length in the limit where the capillary volume vanishes.

Mastrangelo and Hsu[10] predict two configurations in which autoadhered cantilever beams may be found (we will

a)Electronic mail: mpdebo@sandia.gov
b)Electronic mail: tamicha@sandia.gov
Web page: http:/www.mdl.gov/Micromachine

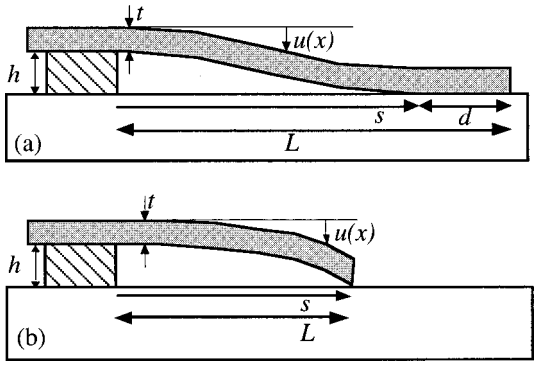

FIG. 1. (a) S-shaped beams ($m=0$) are attached over a long length d. (b) Arc-shaped beams ($m=3/2$) are attached only very near their tips.

subsequently refer to Ref. 10 as MH). Long beams are adhered over a large fraction of their length, and bend into an S shape as in Fig. 1(a). The nonadhered length from the support post to the point at which the beam comes into contact with the substrate is s, and the length of the beam L is significantly greater than s. In this article, we assume a fracture mechanics formalism,[24] and call s the crack length. Alternatively, short adhered beams contact the substrate only at their tip, and the beams assume an arc-shaped deformation as in Fig. 1(b). In this case, the crack length s is very nearly equal to L.

MH argue that either adhesion geometry can be used to extract a quantitative measure of micromachine surface energy. For S-shaped beams, the crack length s can be used to determine the apparent surface energy. However, an out-of-plane measurement technique is required to determine s. Perhaps because such a method is not commonly available in laboratories, MH recommend using the arc-shaped beam. Then, using a high-power objective on an optical microscope, adhesion energy is determined by observing the shortest beam to remain adhered within an array of beams of various lengths. MH demonstrated the shortest adhered beam approach on polysilicon micromachined beams having both hydrophilic and hydrophobic nature. Although their measurements yield surface energy of reasonable magnitude, they were not able to distinguish between hydrophilic and hydrophobic surfaces.

In this article, we examine the adhesion measurement approach proposed by MH in detail. Using interferometry to measure beam deformations point by point, we extend the experimental measurement to include adhesion of S-shaped beams. By taking this approach we directly address the following outstanding questions:

(1) Do the deformations predicted by MH, which are subsequently used to calculate strain energy, match actual beam deflections?

(2) What is the behavior of beams in the transition from the S to the arc shape? How are the equilibria for the S- and arc-shaped beams attained?

(3) Are the values for adhesion between S and arc-shaped beams equivalent? If not, what factors influence measured differences?

II. MECHANICS OF ADHERED CANTILEVER BEAMS

A. Beam deformations

The total energy of the adhered beam is a sum of (a) the elastic energy stored by bending a beam into contact with the substrate, and (b) the surface energy reduction achieved by forming a beam/substrate interface. Solving for the minimum total-energy system allows one to directly determine the equilibrium surface energy. The first step in this approach is a quantitative evaluation of the stored elastic energy in an adhered beam.

In the absence of externally applied forces, the deformations for an adhered beam are given by MH as

$$u(\eta)=h\eta^2\{[m(s)-2]\eta+[3-m(s)]\},\quad \eta=\frac{x}{s}, \tag{1}$$

where h is the height of the support post, t is the thickness of the beam, L is the beam length, and s is the crack length (see Fig. 1). The attachment length d is the length along which the two materials are in contact, and $d\approx L-s$. The slope parameter m is defined by $\theta=m(h/s)$, where θ is the shear angle of the beam tip. From MH, the functional form of m derived from beam shear theory is

$$m(s)=\frac{\frac{16}{5}\left(\frac{t}{d}\right)^3\left(\frac{t}{s}\right)\left[1+\frac{15}{32}\left(\frac{d}{t}\right)^2\left(\frac{E}{G_2}\right)\right]}{1+\frac{32}{15}\left(\frac{t}{d}\right)^3\left(\frac{t}{s}\right)\left[1+\frac{15}{32}\left(\frac{d}{t}\right)^2\left(\frac{E}{G_s}\right)\right]}, \tag{2}$$

where E and G_s are the Young's and shear modulus, respectively. $E/G_s=2(1+\nu)\approx 2.44$, where $\nu=0.22$ is Poisson's ratio for silicon.

For the S-shaped beam, $d\gg t$. Consequently, m approaches zero implying negligible shear deformations at the crack tip s. In the limit when s approaches L, m is a strong function of d, reaching a maximum value of 3/2 for vanishing d. The nonzero slope parameter corresponds to shear deformations induced when adhesive contact is localized to the beam tip.

The assumptions in the MH analysis are: (1) small deformations such that linear elasticity applies; (2) a rigid cantilever support post and substrate; (3) free slip of the beam over the substrate; (4) attractive forces that operate only between contact portions of the beam and substrate surfaces; (5) no residual strain (curvature) in the beam; and (6) perfectly smooth beam and substrate surfaces.

B. Mechanical equilibrium

In this section, we extend the analysis of MH to investigate the mechanical equilibria of the S- and arc-shaped cases. We shall find that the energy well is much deeper for the S-shaped than the arc-shaped deformation and that m can *only* take on values near 0 or near 3/2.

Using the deformation characteristics from the previous section, the elastic strain energy in an adhered beam is given by

$$U_E=\frac{EI}{2}\int_0^s\left(\frac{d^2u}{dx^2}\right)^2dx=\frac{6EIh^2}{s^3}\left(1-m(s)+\frac{m^2(s)}{3}\right), \tag{3}$$

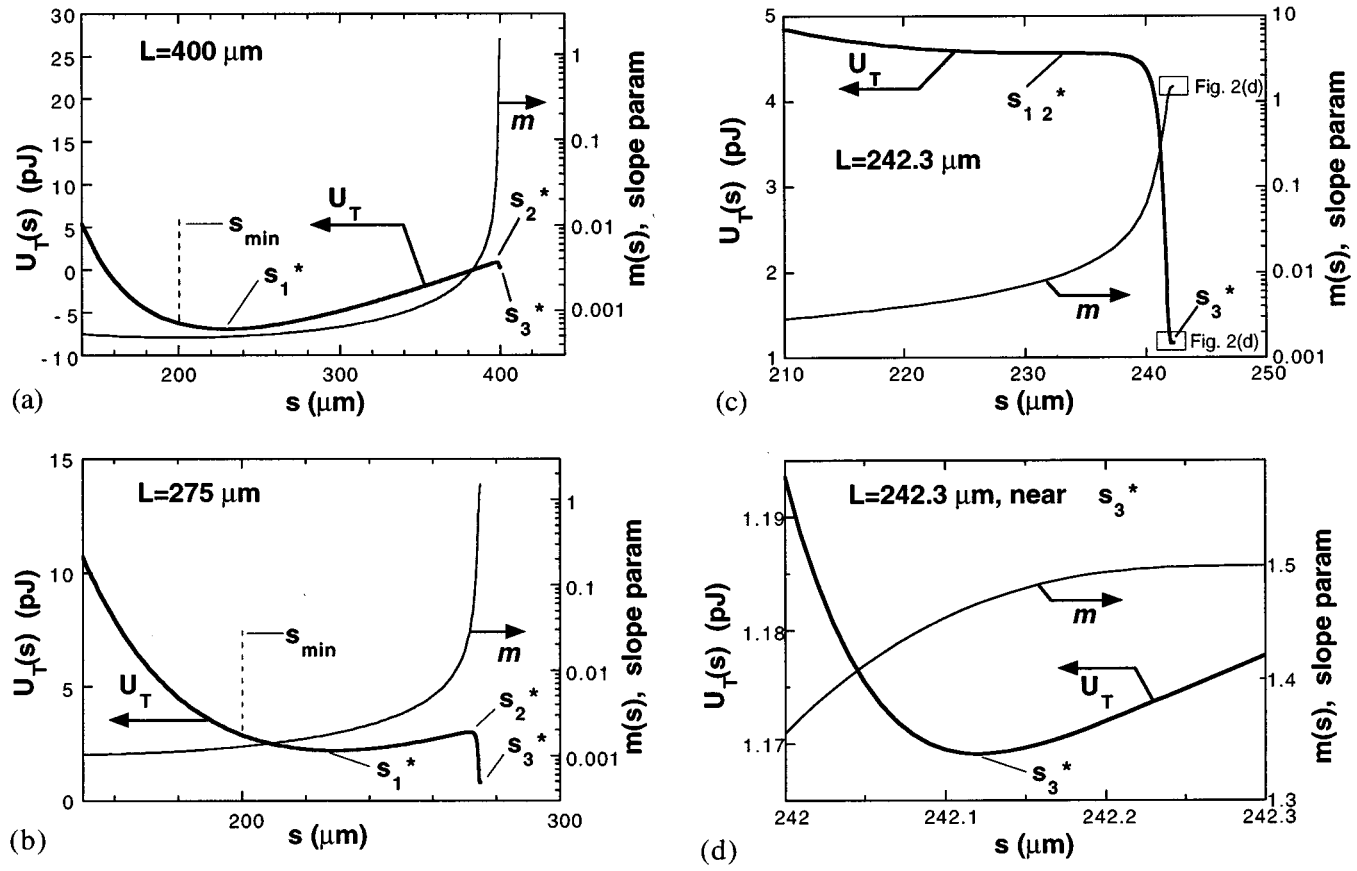

FIG. 2. (a) U_T and m vs s for $L=400$ μm and $\Gamma=3.66$ mJ/m^2. Local minima exist at s_1^* and s_3^*. The minimum in U_T is approximately -7 pJ. (b) At $L=275$ μm, the relative values of U_T at s_1^* and s_3^* have changed. (c) At $L=242.3$ μm, the extrema at s_1^* and s_3^* have merged into s_{12}^*. (d) Close up of (c) in the vicinity of s_3^*. The minimum in U_T at s_3^* is only 10 fJ.

where $I=wt^3/12$ is the beam moment of inertia. Equation (2) shows that as the crack length s decreases, the stored elastic energy increases. The surface energy U_s is

$$U_s=-\Gamma w(L-s), \tag{4}$$

where Γ is the energy of adhesion per unit area. The surface energy term is negative because energy is reduced when surfaces come into contact. For clean smooth surfaces, which are reversibly separated, we expect the adhesion $\Gamma=2\gamma$, where γ is the surface energy of the material in question. Because the beam and substrate are made of the same material, no separate interfacial energy exists and the adhesion energy Γ is simply twice the surface energy. In actual micromachined beams, factors such as surface roughness and capillary condensation must be considered when evaluating the effective surface energy.

The total system energy U_T is the sum of the elastic strain energy and the adhesive surface energy:

$$U_T=U_E+U_S=\frac{6EIwh^2}{s^3}\left(1-m(s)+\frac{m^2(s)}{3}\right)-\Gamma w(L-s). \tag{5}$$

System equilibrium is determined by stable values of U_T defined by

$$\frac{dU_T}{ds}=0, \tag{6a}$$

and

$$\frac{d^2U_T}{ds^2}>0. \tag{6b}$$

To characterize the system equilibrium, we determine stable values of U_T for various length beams assuming a fixed value of Γ. A straightforward method to solving Eq. (6) is by the graphical method. It is necessary to eliminate d from Eq. (2) using $d\approx L-s$. Then, Eq. (2) can be rewritten as

$$m(s)=\frac{A(s)}{1+(2/3)A(s)}, \tag{7}$$

where $A(s)$ is defined in terms of known constants and variable s as

$$A(s)=\frac{16}{5}\left(\frac{t}{L-s}\right)^3\left(\frac{t}{s}\right)\left[1+1.144\left(\frac{L-s}{t}\right)^2\right]. \tag{8}$$

Using Eqs. (5), (7), and (8), we plot in Fig. 2 U_T vs s for various values of L assuming $\Gamma=3.66$ mJ/m^2, $t=2.3$ μm, $h=1.8$ μm, and $w=20$ μm (reflecting the data for hydrophobic samples in Sec. III below). The state in which the system will reside is the lowest *reachable* minimum for U_T after drying. In Appendix A, we estimate two characteristic lengths, $L_{\text{tip},0}$ and $L_{\text{tip},c}$. The former is the minimum length beam which will be brought into contact with the substrate at

an angle of 0° as its tip, while the latter is the shortest beam which will be brought into contact at an angle greater than 0°. The reachable minimum, after drying is complete, depends on the shortest value of $s=s_{\min}$ achieved while external forces pull the beam into contact with the substrate. As seen in Appendix A, this depends on both the surface tension of the liquid as well as its contact angle with the substrate. In this example, we shall take $s_{\min}=L_{\text{tip},0}=200\mu$m for S-shaped beams, reflecting a receding contact angle during the drying process of $\theta_{cr}=80°$.

Figure 2(a) is a graph of U_T and m vs s for $L=400\mu$m. For small s, U_T grows large due to bending strain energy U_E, while m is near 0. Note that m (plotted on a logarithmic scale) is not exactly 0 because the theory accounts for beam shearing at the crack tip, which exists to a small degree even for the S-shaped beam. For large s, U_T increases because surface energy U_S becomes substantial. However, as $s\rightarrow L$, m rapidly begins to increase towards 3/2, reflecting the change from the S to the arc shape. A commensurate decrease in U_E occurs, and is manifested as a local minimum in U_T. Regarding stability, at $s_1^*=229$, $s_2^*=398.2$, and $s_3^*=399.76$ μm, Eq. (6a) is satisfied, but Eq. (6b) is satisfied only at $s_1^*=229$ and $s_3^*=399.76$ μm (s^* refers to the local extrema). The absolute system minimum in U_T of -7 pJ is at $s_1^*=229$ μm with $m=0$. It is approached and reached from the left-hand side because, before drying, $s_{\min}<s_1^*$. The local minimum U_T at $s_3^*=399.76$ μm is not reachable. For long beams such as in Fig. 2(a), the fracture equilibrium is stable due to the relatively deep well of 8 pJ at s_1^*, and is independent of beam length. Note that if $s_{\min}$ were greater than s_1^*, as large as $\sim$390 μm, the same equilibrium would be achieved as the sample dries. Then, the equilibrium is reached from the right, but the same equilibrium is found because of the depth of the energy well around s_1^*.

In Fig. 2(b) the plot is repeated at $L=275$ μm, where important details have changed. The value of $U_T=2.2$ pJ at s_1^* has increased because the relative contribution of the surface energy term $\Gamma w(L-s_1^*)$ has decreased. There are again two values of s^* for which both Eqs. (6a) and (6b) are satisfied, namely, at $s_1^*=229$ and $s_3^*=274.80$ μm. The system minimum is now at s_3^*. It is not reachable from $s_{\min}$ because of the energy barrier of about 0.8 pJ at s_2^* relative to s_1^*. Therefore, the system remains in the local minimum at s_1^* with $m=0$ when drying is complete. The energy well at s_1^* is now much more shallow than in Fig. 2(a), 0.5 pJ. Yet, if $s_{\min}$ were greater than s_1^*, as large as $\sim$270 μm, the same equilibrium would be achieved from the right of s_1^*.

As seen in Fig. 2(c), the local minima at s_1^* and s_2^* merge as L decreases to 242.3 μm. Now there are only two values of s which satisfy Eq. (6a), namely, at $s_{12}^*\approx 233$ μm and $s_3^*=242.12$ μm. Of these, only the latter value satisfies Eq. (6b). The value of $s_{12}^*\approx 233$ μm has increased slightly above the earlier value of $s_1^*=229$ μm at this transition point because the contribution of surface energy continues to diminish. The system minimum at s_3^* is now reachable, but the value of m changes dramatically from nearly 0 to nearly 3/2. The energy well at s_3^* is now exceedingly shallow, only $\sim$0.01 pJ, as can be seen in Fig. 2(d).

The disappearance of the stable minimum at s_1^* implies an abrupt transition in m from 0 to 3/2 as L decreases. Physically, it can be related to the high stored strain energy in the S-shaped beam relative to the arc-shaped beam. Consider the free-body diagram in Fig. 3. To maintain the S shape, a significant moment resulting from the adhesion over the attachment length d develops at the crack tip. When d becomes too short, the beam snaps to the arc shape because it is energetically accessible. The required moment arm reduces to a value very near 0, and d dramatically decreases from 9.3 to 0.2 μm.

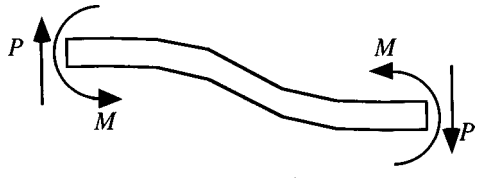

FIG. 3. Free-body diagram for an S-shaped beam. The force and moment are provided by the support post on the left-hand side. On the right-hand side, the moment and tensile force develop due to adhesive forces. When the attachment length d becomes too short, the S shape can no longer be maintained.

As L decreases further, the beam no longer comes into contact at a slope of $m=0$ for $L<L_{\text{tip},0}=200\mu$m. As shown in Appendix A, the tip is still brought into contact for $L>L_{\text{tip},c}=115.6$ μm. Therefore, the beam remains adhered at its tip with $m\approx 3/2$ after the capillary dries. However, at $L=161.9$ μm, the shallow energy well at s_3^* disappears and the attachment length d vanishes. Note that the deflections are equivalent to the case of point loading for arc-shaped beams when $m\rightarrow 3/2$. Therefore, as the capillary drop at the beam tip dries for $L<161.9$ μm, the beam should pop off if the adhesion is equivalent for S and arc-shaped beams.

C. Adhesion

From a fracture mechanics perspective,[24] a crack driving force is derived from the strain energy release rate G defined as

$$G=-\frac{1}{w}\frac{dU}{ds}. \tag{9}$$

Here, the rate refers to changing values of s. The adhesion is determined when the strain energy release rate G equals the crack resistance or adhesion Γ, i.e.,

$$G=\Gamma. \tag{10}$$

This is identical to the condition (6a) above. Combining Eqs. (3) and (10) results in

$$G=\frac{Et^3h^2}{2}\left\{(3s^{-4})\left[\frac{m^2(s)}{3}-m(s)+1\right]+(s^{-3})\frac{dm(s)}{ds}\left[\frac{2m(s)}{3}-1\right]\right\}. \tag{11}$$

Knowing E, t, and h, G can in principle be determined for *any* adhered beam by measuring s, m, and dm/ds. As seen from the discussion of equilibrium above, m can take on values only very near 0 or very near 3/2. For beams adhered

in the S shape, m is slowly varying, and hence, dm/ds can be taken to be 0. Regarding beams adhered in the arc shape, it is difficult to experimentally determine a value for dm/ds. The exception is for the shortest adhered beam in the arc shape, where again, dm/ds is 0. Therefore, practically speaking, an adhesion measurement for arc-shaped beams is only possible for the shortest adhered beam. Hence, the two limiting cases of Fig. 1 give rise to the expressions

$$G=\frac{3}{2}\left(\frac{Et^3h^2}{s^4}\right), \quad \text{for } m=0, \tag{12a}$$

and

$$G=\frac{3}{8}\left(\frac{Et^3h^2}{s^4}\right), \quad \text{for } m=3/2. \tag{12b}$$

Here, Eq. (12a) applied to any beam of sufficient length, while Eq. (12b) applies only to the shortest adhered beam.

S-shaped beams with long attachment length d are always free to approach the equilibrium adhered state; i.e., subsequent to a perturbation on the system which forces s from its equilibrium value, s_1^* can be reached whether $s>s_1^*$, or $s<s_1^*$. In fact, the situation for large d is very similar to Obreimoff's early fracture mechanics experiment[25] in which the fracture energy of mica was determined from interferometric measurements. Note that the situation for Eq. (12b), although most commonly used to report adhesion measurements in micromachining[9,10,15–17,26] or to compare calculations to data,[27,28] is precarious at best. This is because the depth of the energy well, already exceedingly small for the arc-shaped beams, approaches zero for the shortest adhered beam. In other words, the equilibrium for small d is not always accessible; i.e., if s grows to be larger than s_3^*, the beam will pop off and an adhesive equilibrium can no longer be found. We now proceed to the measurement of deformations and equilibrium adhered lengths for a range of cantilever beam geometries.

III. EXPERIMENTAL METHODS AND RESULTS

A. Specimen fabrication and surface treatment

Our micromachined structures were fabricated with one photolithographic mask level. First, an $h=1.8$ μm oxide was deposited on single-crystal ⟨100⟩-oriented silicon. A $t=2.3$ μm layer of polysilicon (as measured by a multiwavelength interferometer) was deposited at 600 °C and then annealed at 1100 °C to relieve residual stresses. Cantilever beams of 20 μm width were defined in an array of increasing L with increments of 2 μm from 10 to 100 μm, and with increments of 5 μm from 100 to 500 μm. The beam support was defined by making the polysilicon wider in this area. The samples were placed in a controlled time HF acid etch such that the oxide under the beams was removed, but remained under the support posts. The samples were next transferred to deionized water, immersed in hydrogen peroxide to form a thin silica layer, and then transferred back to deionized water.

One set of samples was removed from the water and dried in air for two days or more. We shall refer to these as the hydrophilic samples. The other set was treated with a molecular coating of octadecyltrichlorosilane, $CH_3(CH_2)_{17}SiCl_3$ (ODTS). We shall refer to these as the hydrophobic samples. ODTS has been investigated as a promising molecule for minimization of adhesion in MEMS.[8,22,29,30] The head group of the organosilane is hydrolyzable, which facilitates the formation of covalent siloxane bonding to the substrate hydroxyl groups as well as between neighboring silane molecules to form a well-attached organosilane layer.[31] Meanwhile, the CH_3 tail groups exposed to the surface exhibit low surface energy ($\sim$20 mJ/m^2), and are hydrophobic (contact angle $\sim$110°). Following the recipe prescribed in Ref. 22, the specimens were transferred from water to isopropanol to isoctane, a series of solvents for which the next is miscible with the previous. The specimens were next submersed in a 1 mM ODTS solution of 4:1 hexadecane:chloroform for 30 min, during which the ODTS molecules deposit on the polysilicon surfaces. The specimens were then transferred back to the solvents in reverse order, and finally, removed from water and air dried.

B. Measurement procedures

To make quantitative measurements of beam deformations and adhered length, we equipped our Leitz Orthoplan optical microscope with a Michelson interferometric attachment and green light monochromator (547 nm as characterized by spectrum photometry). To ensure minimal error due to tilt, background fringes were aligned parallel with the length of the beams using the tilt adjustment of the reference surface. Interference fringe intensity was recorded with a charge-coupled device camera, and subsequently, analyzed using a standard image processing program.[32] Linescan intensities along the length of adhered beams were converted into u-deflection versus x-position data using a computer program. An absolute deflection accuracy of about 50 nm (across the entire beam), and a relative accuracy (pixels near each other) of about 10 nm resulted. The spatial resolution of our 20× objective was about 1 μm. Measurements of beam height versus distance along the beam were used to assess the adhered beam length and to provide a direct comparison with beam deflections predicted from elasticity theory.

C. Experimental results

1. Hydrophilic beams

Measured deformations and adhered length for a hydrophilic beam of length $L=365$ μm are presented in Fig. 4. Figure 4(a) is an optical interferometric image showing three such adhered beams. Intensity versus position data from a linescan taken along the beam designated by a white line in Fig. 4(a) are plotted in the graph of Fig. 4(b) (right-hand y axis). The beam comes into contact with the substrate at the point where the linescan flattens out, at $x=172.4$ μm ($u=1820$ nm). From the linescan data, u deformations were computed and are plotted as a solid line referenced to the left-hand axis of Fig. 4(b). For comparison, predicted deformations for the extremes of $m=0$ and $m=3/2$, using Eq. (1), are also plotted using dashed lines. It is seen that the actual deformations agree well with those predicted for the case $m=0$, consistent with the S-shaped deformation for beams adhered over a significant fraction of their length. Using

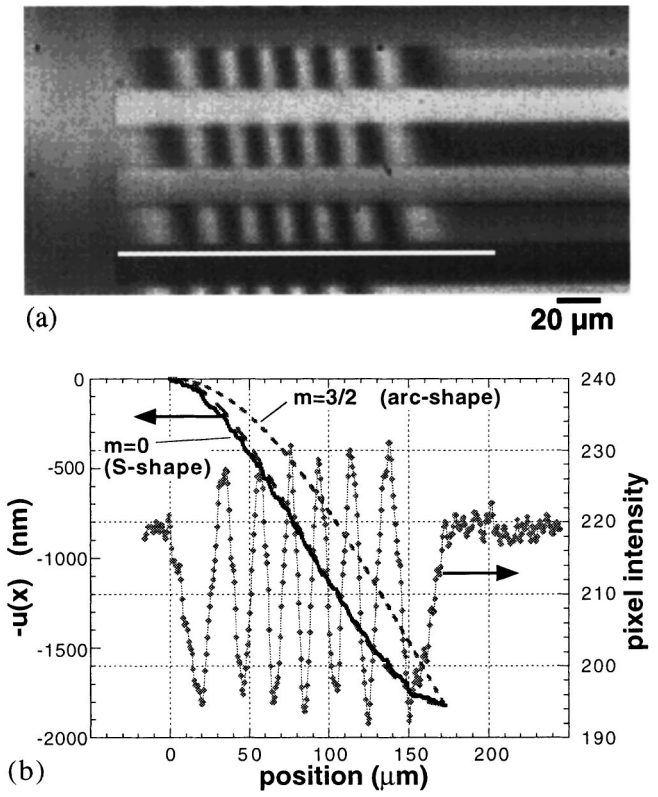

FIG. 4. (a) Interferogram of several long beams subjected to hydrophilic treatment. (b) Linescan across the beam adjacent to the white line of (a), and conversion to $u(x)$ deflections, which compare well with the deflections from MH for S-shaped beams.

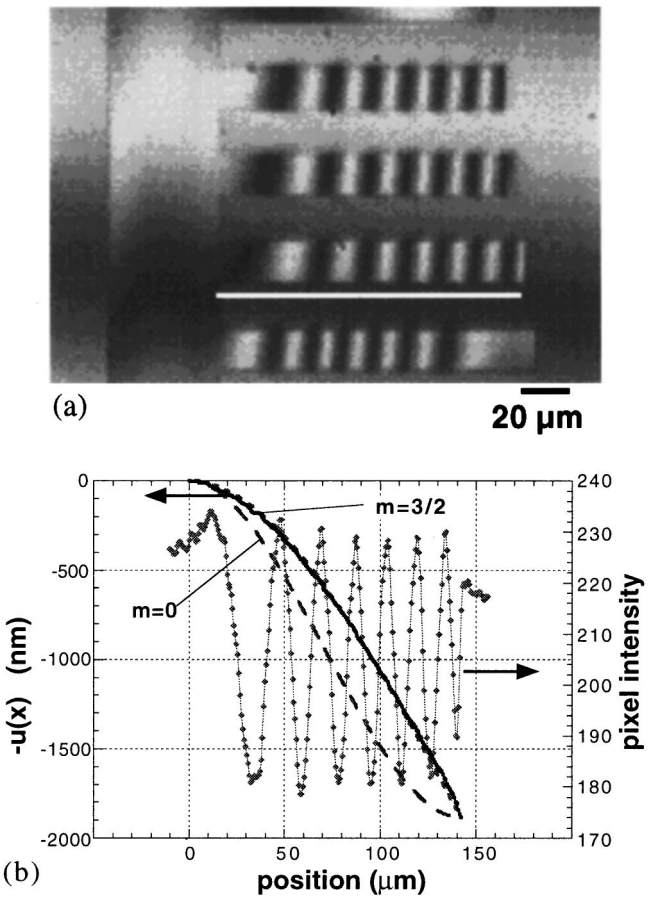

FIG. 5. (a) Interferogram of shorter beams subjected to hydrophilic treatment. (b) Deflections of beam adjacent to the white line compare well with the MH calculations for arc-shaped beams. The beam below remains in the S shape.

measured values of $s_1^* = 172.4$ μm, $h = 1800$ nm, $t = 2.3$ μm, and assuming $E = 170$ GPa,[33] an adhesion value of $\Gamma = 11.3$ mJ/m^2 was calculated using Eq. (12a).

Adhesion measurements on various length beams were made to determine the range over which deformations matched the case $m = 0$. For sufficiently long beams, the agreement was excellent. However, as the beam length approached the value of 175 μm, a transition to the $m = 3/2$ deformation was observed. For beams shorter than 175 μm, the value of m toggled between 0 and 3/2. An example of this behavior is seen in Fig. 5. In the interferometric image of Fig. 5(a), the 140 μm long beam designated by the white lines has fringes out to its tip, indicating an arc-shaped beam geometry. Figure 5(b) shows good agreement with the $m = 3/2$ deformation condition. The 145 μm beam, just below the designated beam, does not have fringes out to its tip. The measured deformation on the 145 μm beam agrees well with the $m = 0$ beam deformation. All beams of less than 145 μm length remain adhered with an arc shape.

The shortest value of L for which beams remained adhered was 58 μm. If Eq. (12b) is used to quantify Γ for this case, the result is that $\Gamma = 222$ mJ/m^2. However, as seen in Fig. 6 (for the case of a 68 μm long beam), the measured deformations lie somewhere between that predicted by the $m = 0$ and $m = 3/2$ limiting conditions. This change in deformation behavior is due to the compliance of the step-up post, which is expected to be non-negligible for beams below 100 μm in this geometry.[34] Compliance in the step-up post reduces the strain energy that is stored in the beam, and hence, the calculation for adhesion according to Eq. (12b) requires a correction. Although a much smaller effect, the step-up post compliance is also nonzero for the case of S-shaped beams, Fig. 4. In Appendix B, we use the measured slope at the beginning of the beam and match the actual beam deformations to account for the step-up post compliance in both the S- and arc-shape cases. The correction decreases Γ from 11.3 to 9.4 mJ/m^2 for the S-shaped beams, and from 222 to 91 mJ/m^2 for the arc-shaped beams. Note that adhesion Γ remains a factor of 10 different even after this correction.

A summary of the results for untreated beams is plotted versus beam length in Fig. 7(a). The left-hand axis displays values of Γ while the measured slope parameter is referenced to the right-hand axis. For long beams in the $m = 0$ condition, the variation in Γ reflects beam-to-beam differences in local adhesion. The average and standard deviation for measured adhesion energies for S-shaped beams are reported in Table I (row 1).

2. Hydrophobic beams

Even though our ODTS-coated beams had a measured contact angle of about 105°, capillary action from drying was still able to pull beams into contact with the substrate. We

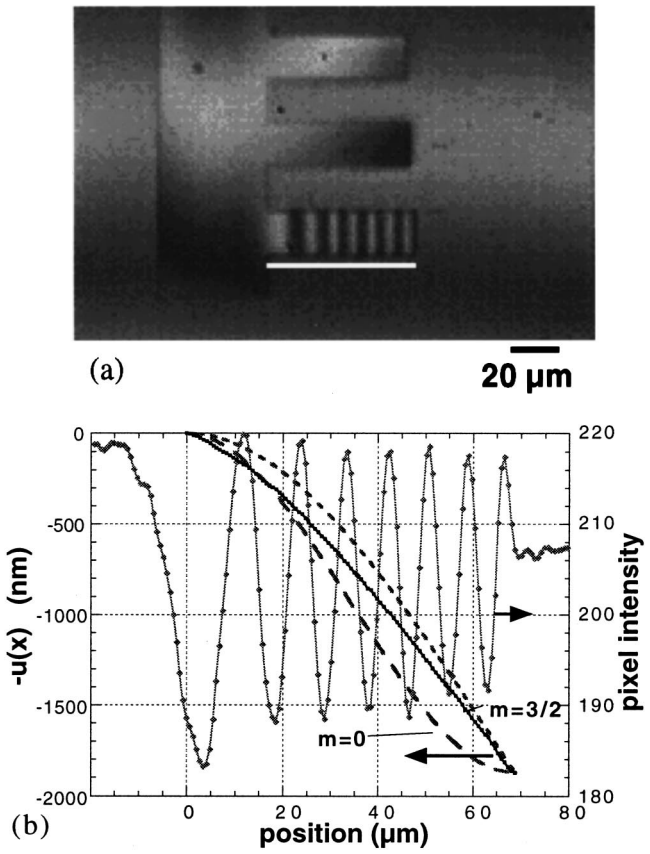

FIG. 6. (a) Interferogram of short beam ($L=68$ μm) subjected to hydrophilic treatment. (b) Deflections which compare poorly with the MH calculations for arc-shaped beams due to significant support-post compliance.

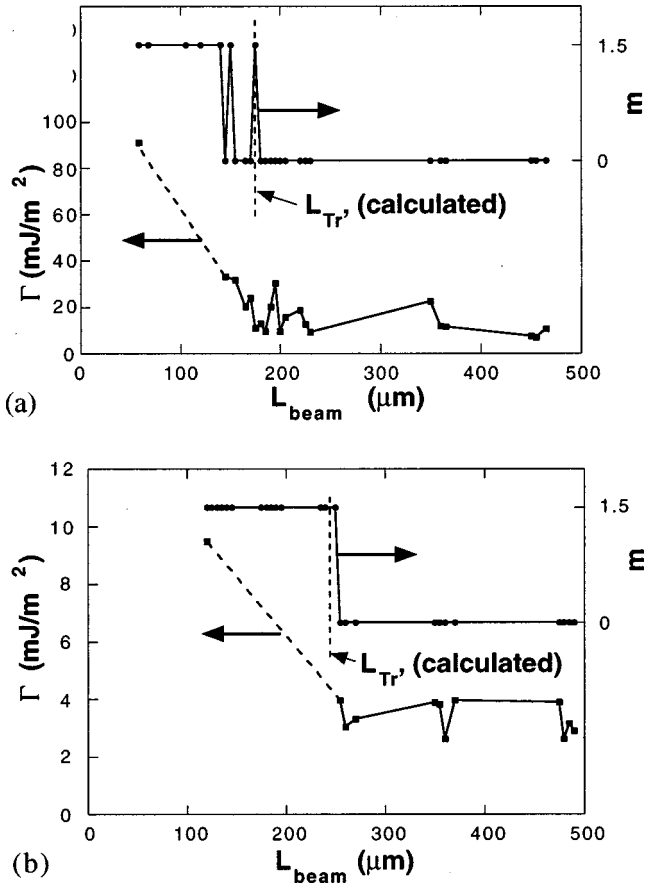

FIG. 7. (a) Adhesion Γ and slope factor m vs beam length L for hydrophilic treatment. The value of the shortest arc-shaped beam is approximately ten times higher than the S-shaped beams. (b) Hydrophobic treatment. The value of the shortest arc-shaped beam is approximately three times higher than the S-shaped beams.

are certain attachment occurred during drying because beams were observed to be free under an optical microscope just before being removed from water. We believe that this result is explained by the observation that *receding* contacting angles are often observed to be smaller than advancing contact angles, a phenomenon known as contact-angle hysteresis.[35] Further confirmation of this stems from an experiment in which we performed video microscopy of drying of previously adhered ODTS beams. This *in situ* drying experiment was conducted without interferometry in order to allow sufficient free-working distance between the water and the microscope objective. Out-of-plane deflections could still be observed because green light is weakly transmitting in polysilicon, giving rise to a weak but observable contrast. Although a drying front of water moving across the surface was observable in one video frame and had disappeared in the next 30 ms later) due to its rapid velocity over the hydrophobic surface, water remained microscopically in the vicinity of the beams for a full second, and clearly pulled the beams further in. ODTS density on the substrate surface is known to be a strong function of deposition conditions.[36] We hypothesize that because the ODTS film did not attain maximum density in our deposition, the adhesion-controlling receding contact angle θ_{cr} was less than 90°.

For long ODTS-treated beams, we observed again excellent agreement with deformations predicted for the $m=0$ condition yielding an s_1^* of 225 μm. This adhesion length corresponds to an adhesion energy of $\Gamma=3.9$ mJ/m^2 using Eq. (12a). By making a correction as reported in Table III, the value is reduced to 3.6 mJ/m^2. The transition from $m=0$ to $m=3/2$ was abrupt at $L=250$ to 245 μm; no toggling between the values of m was apparent. The shortest adhered beam was at $L=120$ μm. Compared to the hydrophilic case, the measured deformation conformed well with the arc shape, indicating that compliance in the step-up post is small. Using Eq. (12b) results in an adhesion value of $\Gamma=12.1$ mJ/m^2. The correction as reported in Table III now reduces Γ only to 9.5 mJ/m^2. Note that this value remains approximately three times larger than that obtained with beams adhered in the S-shaped geometry. The results are summarized in Fig. 7(b), and the average and standard deviation S-shaped beams is tabulated in Table I. Note that the average value of Γ is approximately five times lower for the hydrophobic than the hydrophilic beams.

TABLE I. Γ for S-shaped beams ($m=0$).

Treatment	Γ (mJ/m^2)	σ	σ/Γ
Hydrophilic	16.5	8.2	0.5
Hydrophobic	3.4	0.5	0.16

TABLE II. Values for $L_{\mathrm{tip},c}$ and $L_{\mathrm{tip},0}$ vs θ_{cr}.

θ_{cr}	$L_{\mathrm{tip},c}$ (μm)	$L_{\mathrm{tip},0}$ (μm)
0	74.6	129.3
30	77.4	134.0
60	88.8	153.7
80	115.6	200.3
85	137.4	237.9
89	205.3	355.7
89.9	365.1	632.4
89.99	649.3	1124.6

IV. DISCUSSION

In this section we use our experimental results to address each of the questions that we posed in Sec. I.

(1) Are the predicted beam deflections valid for micromachined beams?

Using interferometry, we have carefully compared actual beam deformations against those assumed in the model of MH. For adhered beams which come into contact with the substrate beyond 120 μm from the support post, we find that the deformations match those of MH quite well. However, we find that the arc-shaped beams with hydrophilic surfaces yield deformations that are considerably different that predicted by the simple model. The explanation is that the deformation model assumes a rigid support post, while the actual micromachined beams have more complex and compliant support-post geometries. In our processing approach, undercutting of the rigid support post occurs during the release etch and contributes additional compliance to the beam structure. In Appendix B, we showed how the effect of compliance could be evaluated. Other fabrication approaches for support posts, such as that used by MH, avoid the undercutting problem but also involve inherently compliant support-post structures.

Our results show that support-post compliance errors increase as the actual adhesion energy increases. This simply reflects the increased torque generated by a larger adhesive force at the adhered end of the beam. Although support-post compliance is most apparent for the shortest adhered beams, close examination of Figs. 4(b) and 5(b) suggests that some support-post compliance may be responsible for the small discrepancy between the measured and predicted deformations in the S-shaped configuration. MH suggest that the effect of support-post compliance on the measured adhesion energy can be removed by plotting the detachment length as a function of beam dimensions. In order to implement this approach one must independently vary the support-post height and beam thickness. However, the processing modifications needed to independently vary the beam dimensions are difficult to achieve and may themselves lead to intrinsic changes in the curvature of the polysilicon or surface roughness that can also influence the measured adhesion energy. For this reason it is best to directly confirm the nature of deflections of the adhered beams and make corrections which account for the step-up post compliance. We have carried out this procedure as outlined in Appendix B.

TABLE III. Corrected values of Γ.

Treatment	Beam shape	s (μm)	Uncorrected Γ (mJ/m^2)	Corrected Γ (mJ/m^2)
Hydrophilic	Arc	58	222	91
	S	172	11.3	9.4
Hydrophobic	Arc	120	12.1	9.5
	S	225	3.9	3.6

(2) What is the behavior of beams in the transition from the S shape to the arc shape? How are the equilibria for the S- and arc-shaped beams attained?

The equilibrium mechanics in Sec. II B suggest that there should be an abrupt transition length L_{Tr} at which the transition from S- to arc-shaped beams occurs. The values of L_{Tr} can be determined quantitatively by carrying out the exercise in Sec. II B, based on knowing the value of Γ for S-shaped beams. For the hydrophilic case, we calculate $L_{\mathrm{Tr}}=174.5$ μm, while as shown in Sec. II B, $L_{\mathrm{Tr}}=242.3$ μm for the hydrophobic case. Figure 7 confirms that this behavior is observed experimentally, and is in excellent quantitative agreement with the calculations for L_{Tr}. For the hydrophilic films, the transition length occurs from 180 to 140 μm, while for the hydrophobic beams the transition occurs from 250 to 245 μm. The larger range of the transition observed experimentally in the hydrophilic compared to the hydrophobic case is due to larger local differences in adhesion. Note that the ratio of standard deviation to average adhesion for S-shaped beams, σ/Γ, is 0.45 for the hydrophilic beams versus 0.16 for the hydrophobic beams. Because the ratio approaches one half, it is not surprising to observe that the transition length varies in the hydrophilic case. Hence, a nonabrupt value of L_{Tr} indicates that adhesion is not well controlled locally.

How are the equilibria for the S- and arc-shaped beams attained? For the hydrophilic case, the shortest beam attached is 58 μm. According to the calculations outlined in Appendix B, this beam is effectively 73 μm long when the step-up post compliance is considered. Therefore, from Table II the receding contact angle θ_{cr} of the drying water must be near 0° in the hydrophilic case, because then $L_{\mathrm{tip},c}\sim 75$ μm. Furthermore, from Table II, for $\theta_{cr}=0°$, $L_{\mathrm{tip},0}\sim 130$ μm. Recall that $L_{\mathrm{Tr}}=174.5$ μm for this case. We hypothesize the following occurs during the drying process: Long beams with $L>L_{\mathrm{Tr}}$ are pulled in to a value $s_{\min}\sim L_{\mathrm{tip},0}=130$ μm when the capillary exerts its maximum force. Because adhesion energy $\Gamma=10$ mJ/m^2 is much smaller than $2\gamma\cos(\theta_{cr})=146$ mJ/m^2, surface energy exerts only a weak subsequent effect, and therefore, $s_{\min}$ is only slightly less than $L_{\mathrm{tip},0}$. However, because $s_1^*=172.4$ μm, the equilibrium is approached from the left as the liquid dries (i.e., $s_{\min}<s_1^*$). Intermediate length beams with $L_{\mathrm{Tr}}>L>L_{\mathrm{tip},0}$ are also pulled into the S shape by capillary action. The beam gradually reverts to the arc shape as the capillary dries, because capillary forces remaining over part of the beam will keep it in contact with the substrate. Finally, for short beams with $L<L_{\mathrm{tip},0}$, the beam never attains the S shape. These remain adhered at their tip, however, as drying

progresses. In effect, any beam which contacts the substrate as its tip remains in contact. This is equivalent to the assertion by Abe and Reed.[13] To confirm this hypothesis, *in situ* drying experiments under interferometric conditions are required.

For the hydrophobic case, θ_{cr} is at most 82° from Table II, such that beams of length $L=120$ μm are pulled into contact with the substrate. Therefore, $L_{\text{tip},0}\sim 210$ μm. Surface energy due to capillary force is now $2\gamma\cos(\theta_{cr})=20$ mJ/m^2. This remains larger than surface energy $\Gamma=3$ mJ/m^2, $s_{\min}$ is again only slightly less than $L_{\text{tip},0}$. The drying sequence is qualitatively similar to the hydrophilic case for the long, medium, and short length beams.

(3) Are the values for adhesion between S- and arc-shaped beams equivalent? If not, what factors influence measured differences?

Using corrections as outlined in Appendix B, we were able to directly compare the adhesion energy as determined by the conventional shortest attached beam method and by our adhered length approach. We found a significant discrepancy between the results produced by the two methods, factors of 10 and 3 for the hydrophilic and hydrophobic cases, respectively. Therefore, the values measured by the two methods *are not equivalent*. Before we address differences between measurement approaches, it is important to understand the absolute values obtained. For this purpose, we consider the hydrophilic samples that were treated only with hydrogen peroxide before drying from DI water. This treatment results in beam and substrate surfaces that are covered by a thin layer of hydrophilic SiO_2. In a previous report,[37] we showed that the adhesion energy for silica-covered surfaces is controlled by the inherent roughness of the polysilicon. For perfectly smooth, wetted surfaces one predicts and measures[38] an adhesion energy that is twice the surface energy of water ($\gamma_{\text{water}}=73$ mJ/m^2), or about 146 mJ/m^2. In the case of rough surfaces, the apparent adhesion can be more than an order of magnitude lower due to the limited area of actual contact between surface asperities, and the adhesion increases exponentially with relative humidity.[37] This helps us to understand why Γ is much lower than $2\gamma_{\text{water}}$ for the hydrophilic beams. Of course, at saturation humidity conditions liquid is expected to fill the entire region surrounding individual asperities and lead to adhesion values comparable with smooth surface conditions.

Because surface roughness can play a significant factor in the apparent adhesion energy, one might ask whether the differences observed between measurement techniques may also be due to factors associated with surface roughness. The fact that the actual surface roughness was the same for all beams argues against this notion. However, the contact geometry is quite different for the S- and arc-shaped beams. S-shaped beams make contact with the substrate over a length that is large compared with the scale of the surface roughness. Such a geometry closely approximates the parallel contact of extended surfaces that has been the topic of previous studies of rough surface contact.[39] When the area of contact is much greater than the scale of roughness, it is appropriate to use a statistically averaged measure of surface topography. Alternatively, arc-shaped beams make contact only over microscopic lengths. As seen in Fig. 2(d), a beam which has just made the transition from the S to the arc shape is adhered over ~200 nm. However, the shortest arc-shaped beams will be adhered only over a few tens of nanometers according to the MH calculations. The atomic force microscope linescan in Fig. 8 shows that the period of major asperity peaks on these surfaces (~1 μm) is greater than the predicted length of contact at the tip of the beam. In this situation it is clear that statistical models for true contact area will not be reliable. Given this large difference in contact geometries for the two measurement approaches, it is not hard to believe that the actual contact in the vicinity of the crack tip will also be significantly different for each beam. This actual contact area cannot be explored through direct measurement techniques. It will be interesting in the future to apply numerical techniques such as those developed by Tian and Bhushan[40,41] to model the actual area of contact for the two contact geometries. Perhaps such estimates could help quantify the effect of roughness on a real contact.

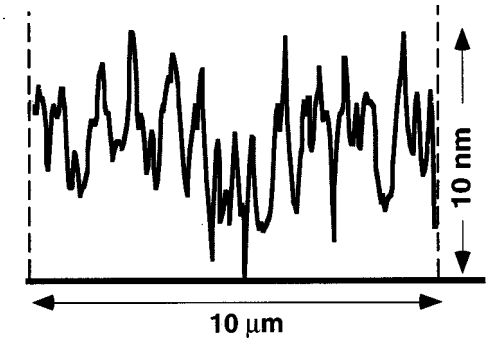

FIG. 8. Atomic force microscope linescan of the bottom side of a polysilicon cantilever beam.

A second effect that may also contribute to the observed difference between apparent adhesion values is related to the drying process itself. As water evaporates from the contact region of arc-shaped beams, impurities will necessarily concentrate in the capillary drop at the tip of the beam. In the limit as the capillary volume vanishes, impurities or solubility products may actually precipitate and lead to the possible formation of a porous solid network in the vicinity of the tip of the beam. Previous fracture mechanics measurements[42] have shown that precipitation of soluble silicates can support stress across solid silicate interfaces. In this scenario, the effective contact area can become much larger than the calculated value leading to an overestimate of the surface energy. Again, the extremely small contact region in the arc-shaped beam makes this measurement approach very sensitive to the nature and size of the contact region. Alternatively, S-shaped beams with their extended adhesive interface are expected to be much less sensitive to such effects.

While the S-shaped beam gives a more reliable value of adhesion than the arc-shaped beam, the latter is of great practical significance. This is because the shortest beam to adhere will always limit the use of MEMS devices. Two-dimensional meniscus effects on the sticking of arc-shaped beams were discussed in Refs. 13 and 14. Narrow-width arc-shaped beams are less likely to stick than wide arc-shaped beams, possibly due to meniscus effects.[43] More work will

be necessary to elucidate the full three-dimensional nature of capillary drying and its interplay with adhesion.

V. SUMMARY AND CONCLUSIONS

We have explored in detail the deformations and adhesive equilibria of micromachined cantilever beams. Our summary and conclusions are as follows:

(1) The deformations for adhered beams were measured by interferometry for arc- and S-shaped beams, and found to agree to first order with the elasticity calculations of MH. This verifies that for long beams (>120 μm for our geometry), the strain energies calculated by MH are appropriate in making adhesion calculations. Discrepancies were significant for adhered beam lengths less than 120 μm, and could be explained and modeled by nonzero support-post compliance.

(2) An abrupt transition from an S- to an arc-shaped beam as L decreases was predicted theoretically, and observed experimentally. This is explained by the disappearance of a local minimum at s_1^* of total system energy U_T as L is decreased. Excellent agreement between calculations and experiment for the transition length L_{Tr} was obtained by using the value for adhesion Γ for S-shaped beams. This suggests that the value of Γ for S-shaped beams controls the transition length, rather than the value of Γ for arc-shaped beams.

(3) Adhesion is best measured on S-shaped cantilever beams which impose a deep energy well and good fracture mechanics equilibrium. When compared to the method of determining the shortest adhered beam in an array of beams with a high-power objective, measurement of a single S-shaped beam by interferometry permits a much smaller area to be occupied to obtain adhesion values. This is valuable because of the expense of real estate area in a MEMS device. S-shaped beams also provide much higher resolution on adhesion than the method of determining the shortest adhered beam. Adhesion statistics are obtained in a straightforward manner by measuring several S-shaped beams in close proximity.

(4) The apparent adhesion calculated for the shortest arc-shaped beam can be different from the adhesion for S-shaped beams. The probable reason is that the attachment length d for arc-shaped beams, calculated from beam theory but impossible to confirm experimentally, is incorrect. Due to statistical variations in roughness, the contact area sampled by the crack tip of the arc-shaped beam may be smaller or larger than that sampled by the crack tip of the S-shaped beam. If the beam is dried from a liquid environment in which capillary action has brought it in contact with the substrate, the effective contact area is very likely larger than the calculated value, giving rise to an anomalously high value of adhesion.

We have demonstrated that the S-shaped cantilever beam configuration should be adopted for detailed studies of adhesion forces in surface micromachining. This method gives great latitude in measuring autoadhesion because the equilibrium is deep and easily attainable from either side of the equilibrium. Studies such as the effect of environment on autoadhesion are readily adapted to this method.[37] With interferometry, the crack length s is well resolved, and therefore, adhesion is accurately assessed. While surface micromachined structures were used as test samples here, S-shaped cantilever beams may be used to appropriately measure adhesion at smaller and larger scales.

ACKNOWLEDGMENTS

Sandia National Laboratories is a multiprogram laboratory operated by Sandia Corporation, a Lockheed-Martin Company, for the United States Department of Energy under Contract No. DE-AC04-94AL85000. The authors thank Peggy Clews and Tom Gugliotta and the entire staff at the Microelectronics Development Laboratory at Sandia National Laboratories for preparing the samples.

APPENDIX A: DETERMINATION OF CHARACTERISTIC BEAM LENGTHS $L_{\mathrm{tip},0}$ AND $L_{\mathrm{tip},c}$

Capillary action exerts negative pressure on a beam as seen in Fig. 9. A complete understanding of the drying problem requires a three-dimensional analysis[13] and is beyond the scope of this work. However, a reasonable analysis for characteristic beam lengths for the case $w \gg h$ from which we can gain some insight into the strength of the capillary liquid is provided in this appendix.

For a given capillary force, we wish to determine the length of the shortest beam, $L_{\mathrm{tip},0}$, for which the beam tip makes a shear angle $\theta=0$ at some point during the drying process. For any beam of length greater than $L_{\mathrm{tip},0}$, surface energy will cause the crack length to become shorter than $L_{\mathrm{tip},0}$ during the drying process. Beams shorter than $L_{\mathrm{tip},0}$ cannot reach the S-shaped configuration. We need to solve for the beam deflection when the capillary extends from the support post to the tip of the beam. In this situation, the beam is uniformly loaded by a force q, as in Fig. 9. A point reaction P at the beam tip opposes this force, Fig. 9.

From the beam theory, the beam is in contact with the substrate if

$$w(L)=\frac{qL^4}{8EI}-\frac{PL^3}{3EI}=h, \tag{A1}$$

and is at an angle $\theta=0$ at its tip if

$$\frac{qL^3}{6EI}-\frac{PL^2}{2EI}=0. \tag{A2}$$

From Eq. (A2), $P=qL/3$, and from Eq. (A1), $q=72hEI/L^4$. Therefore, the shortest beam which will be brought into contact to the substrate with an angle $\theta=0$ at its tip is at

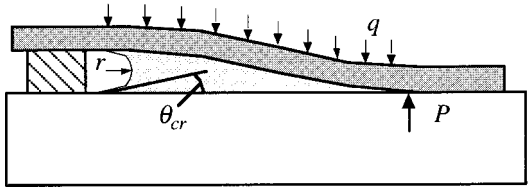

FIG. 9. Forces on the beam during the liquid drying process.

$$L_{\text{tip},0}=\left(\frac{72EIh}{q}\right)^{1/4}. \tag{A3}$$

Likewise, the shortest beam which will be brought into contact at its tip with an angle $\theta>0$ is at $L_{\text{tip},c}$, where

$$L_{\text{tip},c}=\left(\frac{8EIh}{q}\right)^{1/4}. \tag{A4}$$

The uniform loading q is calculated from the Laplace pressure $q/w=\gamma/r$, where γ is the surface tension of the liquid, and r is the radius of the drop in Fig. 9. It is a simple geometrical exercise to show that $r=(h/2\cos\theta_{cr})$, where θ_{cr} is the receding contact angle of water with the solid. Therefore,

$$q/w=2\gamma\cos\theta_{cr}/h. \tag{A5}$$

Finally,

$$L_{\text{tip},0}=\sqrt{3}\,L_{\text{tip},c}=\left(\frac{Et^3h^2}{3\gamma\cos\theta_{cr}}\right)^{1/4}. \tag{A6}$$

In Table II, we give some calculated lengths for $L_{\text{tip},0}$ and $L_{\text{tip},c}$. The values $E=170$ GPa, $\gamma=\gamma_{\text{water}}=73$ mN/m, $w=20$ μm, $h=1.8$ μm, and $t=2.3$ μm are assumed.

The analysis here provides an upper bound for $L_{\text{tip},0}$ and $L_{\text{tip},c}$. In reality, factors such as support-post compliance and edge effects (such as the ''inside meniscus''[13]) will reduce these values somewhat. Considering that in our experiments $w=11h$, the effect of the ''inside meniscus'' will be small.

APPENDIX B: CORRECTING THE VALUES OF Γ FOR SUPPORT-POST COMPLIANCE

Knowing the deflections for the beams, we can take into account the compliance of the step-up support post to improve the values of Γ. This is done by relaxing the constraint that the constants of integration used to derive the deflection curve Eq. (1) be zero. In these calculations, the 15 μm length of the support post was taken into account. The fact that this region was approximately twice as wide as the beam was also considered. The nonzero slope of the beam from the edge of the support post was set to the experimental value. Assigning the proper nonzero constants of integration, we matched the experimental deflections to calculated deflections. From this, the strain energy, and hence, the corrected values of Γ were determined. The results are given in Table III. As expected, the values of Γ corrected for the support-post compliance are smaller than the uncorrected values. For the arc-shaped beam with the hydrophilic treatment, the correction is approximately a factor of 2. However, for the other cases, the correction is 30% or less. This is to be expected considering that only the former deviates significantly from the ideal deflections.

[1] C. H. Mastrangelo and W. C. Tang, in *Semiconductor Sensors*, edited by S. M. Sze (Wiley, New York, 1994), p. 70.
[2] F. Goodenough, Electronic Design **8**, 45 (1991).
[3] P. F. Vankessel, L. J. Hornbeck. R. E. Meier, and M. R. Douglass, Proc. IEEE **86**, 1687 (1998).
[4] E. J. J. Kruglick and K. S. J. Pister, Hilton Head '98, Hilton Head Island, SC, June 8–11, 1998, pp. 333–337.
[5] J. A. Geen, Hilton Head '98, Hilton Head Island, SC, June 8–11, 1998, pp. 51–54.
[6] V. Aksyuk *et al.*, Hilton Head '98, Hilton Head Island, SC, Jun 8–11, 1998, pp. 79–82.
[7] M. S. Rodgers and J. J. Sniegowksi, Hilton Head '98, Hilton Head Island, SC, June 8–11, 1998, pp. 144–149.
[8] R. L. Alley, G. J. Cuan, R. T. Howe, and K. Komvopoulos, Hilton Head (1992), p. 202.
[9] R. L. Alley, P. Mai, K. Komvopoulos, and R. T. Howe, Proceedings of the International Conference on Solid-State Sensors and Actuators (Transducers '93) (1993), p. 288.
[10] C. H. Mastrangelo and C. H. Hsu, Hilton Head (1992), p. 208.
[11] C. H. Mastrangelo and C. H. Hsu, J. Microelectromech. Syst. **2**, 33 (1993).
[12] C. H. Mastrangelo and C. H. Hsu, J. Microelectromech. Syst. **2**, 44 (1993).
[13] T. Abe, W. C. Messner, and M. L. Reed, J. Microelectromech. Syst. **4**, 66 (1995).
[14] T. Abe and M. L. Reed, J. Micromech. Microeng. **6**, 213 (1996).
[15] R. Legtenberg, J. Elders, and M. Elwenspoek, Proceedings of the International Conference on Solid-State Sensors and Actuators (Transducers '93) (1993), p. 298.
[16] M. R. Houston, R. T. Howe, and R. Maboudian, J. Appl. Phys. **81**, 3474 (1997).
[17] Y. Yee, K. Chun, and J. D. Lee, Proceedings of the International Conference on Solid-State Sensors and Actuators (Transducers '95) (1995), p. 206.
[18] R. Maboudian and R. T. Howe, J. Vac. Sci. Technol. B **15**, 1 (1997).
[19] C. H. Mastrangelo, Tribol. Lett. **3**, 223 (1997).
[20] G. T. Mulhern, D. S. Soane, and R. T. Howe, Proceedings of the International Conference on Solid-State Sensors and Actuators (Transducers '93) (1993), p. 296.
[21] M. R. Houston, R. T. Howe, K. Komvopoulos, and R. Maboudian, Mater. Res. Soc. Symp. Proc. **383**, 391 (1995).
[22] M. R. Houston, R. Maboudian, and R. T. Howe, Hilton Head '96, Hilton Head Island, SC, June 3–6, 1996, pp. 42–47.
[23] P. F. Man, B. P. Gogoi, and C. H. Mastrangelo, Proc. IEEE MEMS (San Diego) (1996), p. 55.
[24] H. L. Ewalds and R. J. H. Wanhill, *Fracture Mechanics* (Edward Arnold and Delftse Uitgevers Maatschapij, London, 1991), pp. 82–84.
[25] J. W. Obreimoff, Proc. R. Soc. London, Ser. A **A127**, 290 (1930).
[26] U. Srinivasan, M. R. Houston, R. T. Howe, and R. Maboudian, Proceedings of the International Conference on Solid-State Sensors and Actuators (Transducers '97) (1997), Vol. 2, p. 1399.
[27] K. Komvopoulos and W. Yan, J. Tribol. **119**, 391 (1997). Note: theoretical adhesion calculations in this reference and the next assume that the critical stiffness of arc-shaped beams is determined by a 1 μm contact zone, while the true zone length is vanishingly small.
[28] K. Komvopoulos and W. Yan, J. Tribol. **120**, 808 (1998).
[29] K. Deng, R. J. Collins, M. Mehregany, and C. N. Sukenik, J. Electrochem. Soc. **142**, 1278 (1995).
[30] U. Srinivasan, M. R. Houston, R. T. Howe, and R. Maboudian, J. Microelectromech. Syst. **7**, 252 (1998).
[31] D. L. Angst and G. W. Simmons, Langmuir **7**, 2236 (1991).
[32] Analysis performed using the public domain NIH image program, available from the NIH Image Web site (http://rsb.info.nih.gov/nih-image/).
[33] W. N. Sharpe, R. Vaidyanathan, B. Yuan, G. Bao, and R. L. Edwards, J. Vac. Sci. Technol. B **15**, 1599 (1997).
[34] Q. Meng, M. Mehregany, and R. L. Mullen, J. Microelectromech. Syst. **2**, 128 (1993).
[35] J. Israelachvili, *Intermolecular and Surface Forces* (Academic, New York, 1992).
[36] M. E. McGovern, K. M. R. Kallury, and M. Thompson, Langmuir **10**, 3607 (1994).
[37] M. P. de Boer, P. J. Clews, B. K. Smith, and T. A. Michalske, Mater. Res. Soc. Symp. Proc. **518**, 131 (1998).
[38] T. A. Michalske and E. R. Fuller, J. Am. Ceram. Soc. **68**, 586 (1985).
[39] J. A. Greenwood and J. B. P. Williamson, Proc. R. Soc. London, Ser. A **295**, 300 (1966).
[40] X. F. Tian and B. Bhushan, J. Phys. D: Appl. Phys. **29**, 163 (1996).
[41] X. Tian and B. Bhushan, J. Tribol. **118**, 33 (1996).
[42] B. C. Bunker and T. A. Michalske, in *Fracture Mechanics of Ceramics*, edited by R. C. Bradt, A. G. Evans, D. P. H. Hasselman, and F. F. Lange (Plenum, New York, 1986), Vol. 8, pp. 391–411.
[43] C. J. Kim, J. Y. Kim, and B. Sridharan, Sens. Actuators A **64**, 17 (1998).